Source model of the 2007 Noto-Hanto earthquake (M_w 6.7) for estimating broad-band strong ground motion

Susumu Kurahashi[1], Kazuaki Masaki[2], and Kojiro Irikura[3]

[1]*Graduate School of Engineering, Aichi Institute of Technology*
[2]*Faculty of Engineering, Aichi Institute of Technology*
[3]*Disaster Prevention Research Center, Aichi Institute of Technology*

(Received July 2, 2007; Revised November 13, 2007; Accepted November 22, 2007; Online published February 19, 2008)

A source model for estimating broad-band ground motions from the 2007 Noto-Hanto earthquake (M_w 6.7) is estimated from a comparison of the observed records of the mainshock and synthesized motions based on the characterized asperity model using the empirical Green's function method. The observed records of aftershocks used as the empirical Green's functions are carefully selected to have almost the same radiation characteristics and source distance as the asperities of the mainshock. The best-fit source model consists of two asperities of different size. A large one is located just above the hypocenter, with an area of 6.3×6.3 km^2 and stress drop of about 26 MPa. A smaller one is located north-east of the large one, with an area of 3.6×3.6 km^2 and stress drop of about 10 MPa. The stress drop of the large one is about twofold higher than the average values of inland crustal earthquakes so far estimated, while that of smaller one is almost average. We found that the remarkable directivity pulses from the source model struck the northern part of the Noto peninsula, causing heavy damage in some towns there.

Key words: Broad-band strong ground motion, empirical Green's function method, 2007 Noto-Hanto earthquake, selection of aftershock records as EGF, source model.

1. Introduction

The 2007 Noto-Hanto earthquake ($M_w = 6.7$) at 9:41:58 (JST) on March 25, 2007 occurred west off the Noto peninsula, Japan. Strong ground motions with a Japan Meteorological Agency (JMA) seismic intensity of 6-upper struck Wajima, Anamizu, and Nanao in the northern part of the Noto peninsula, causing one death, about 300 collapsed houses and about 2000 partially destroyed houses (Fire and Disaster Management Agency, 2007). According to Centroid moment tensor (CMT) solutions of National Research Institute for Earth Science and Disaster Prevention (NIED), this earthquake has a compressional axis on the strike of 58°, reverse fault with 66° and rake angle of 132° (NIED, 2007). The distributions of aftershocks indicate that the main fault should be about 25–30 km long and 10–15 km wide (Earthquake Research Institute, 2007). The projections of aftershocks on the cross-sections imply that the fault inclination is almost consistent to the CMT solutions. The earthquake fault was associated with known active faults just off the west shore of the northern part of the Noto peninsula (Katagawa *et al*., 2005). This fault dips beneath the Noto peninsula, which is consistent to the aftershock distributions and the CMT solutions. This might be one of reasons why the damaged areas extended widely over the northern Noto peninsula, which is located on the hanging wall side of the fault. Another reason might be related to the rupture process of this earthquake, such as directivity effects. The source models for estimating broad-band ground motions from large inland crustal earthquakes to date were successfully estimated from a comparison between the observed and synthesized ones based on the characterized asperity model using the empirical Green's function method (e.g. Kamae and Irikura, 1998; Miyake *et al*., 2003). The strong motion generation areas are found to coincide approximately with asperity areas, where a lot of stress is released. In this paper, we attempt to examine whether the above relations are available for modeling the rupture process of the 2007 Noto-Hanto earthquake. It is one of the most important issues associated with increasing the reliability of strong motion prediction and risk assessment for future large earthquakes.

2. Ground Motion Data

We used strong motion data at six observation stations of K-NET installed by NIED (ISK001, ISK002, ISK003, ISK004, ISK005 and ISK006) in the northern region of the Noto peninsula. The locations of the K-NET stations are shown in Fig. 1, together with the mainshock and two aftershocks used for analysis, respectively. The seismic moments and focal mechanisms of the mainshock and aftershocks were determined from the F-net by NIED (NIED, 2007). The source area of each aftershock is estimated from the corner frequency of the source spectrum calculated using the records of the aftershock. The stress drop of the aftershock is inferred from the seismic moment and source area of it. The source parameters mentioned above

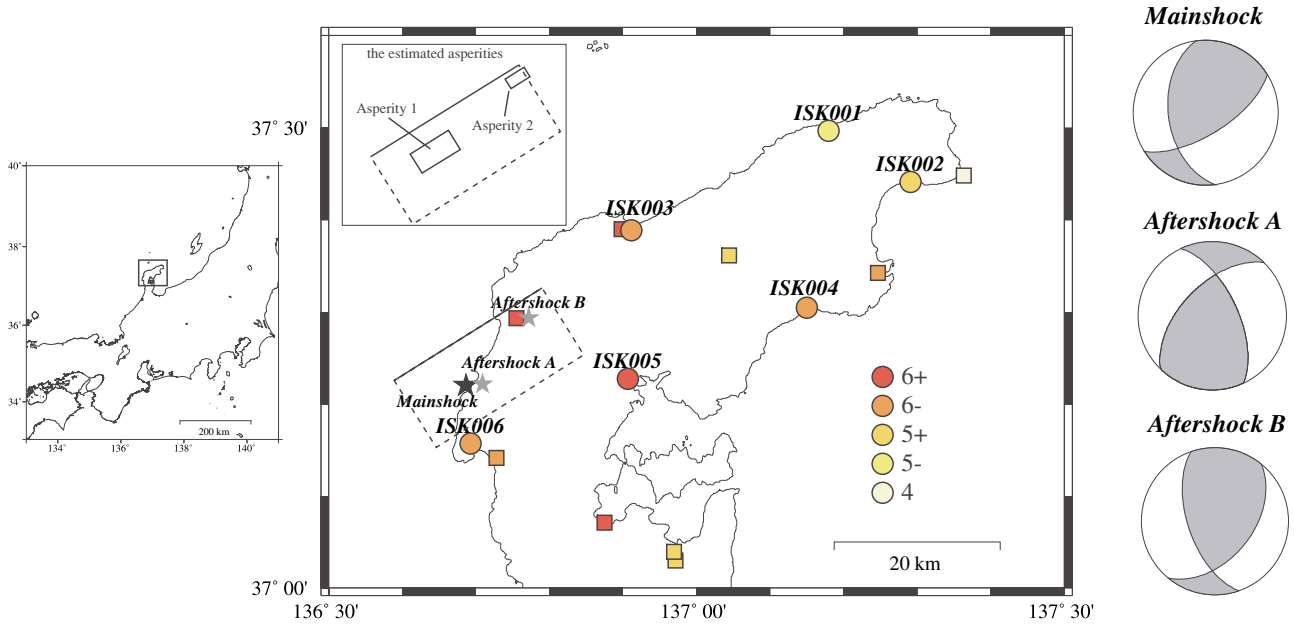

Fig. 1. Map showing the location of stations used for analysis (circle), the other stations (square) and epicenters of the mainshock and aftershocks (star). The JMA seismic intensity in each station is plotted with color markings. The focal mechanisms of the mainshock and aftershocks by F-net (NIED, 2007) are shown in the right.

Table 1. The source parameters of the mainshock, Aftershock A and Aftershock B. Fault area and stress drop of the aftershocks are noted for those before and after the grid search.

	Mainshock	Aftershock A	Aftershock B
Origin time (JST)	2007/3/25 09:42	2007/3/28 08:08	2007/3/25 15:43
Latitude (°)*	37.221	37.222	37.294
Longitude (°)*	136.686	136.709	136.772
Depth (km)*	10.7	13.3	8.9
M_w **	6.6	4.6	4.0
Strike (°)**	58/173	335/225	161/40
Dip (°)**	66/48	62/56	60/48
Rake (°)**	132/34	39/146	51/137
Seismic moment (N*m)**	1.36×10^{19}	1.03×10^{16}	1.25×10^{15}
Fault area (km^2) (before the grid search)	—	2.2	1.0
Stress drop (MPa) (before the grid search)	—	7.6	3.0
Fault area (km^2) (after the grid search)	—	—	0.81
Stress drop (MPa) (after search model)	—	—	4.1

*estimated by JMA, **estimated by F-net.

are shown in Table 1. The analyzed range of frequency was from 0.2 to 10 Hz.

3. Selection of Aftershock Records as Empirical Green's Functions

Some records from aftershocks within the source area of the mainshock have been obtained. The conditions for the aftershock records usable as the empirical Green's functions are as follows: (1) the hypocenter of the aftershock should be near the asperity of the mainshock; (2) the radiation characteristics of the aftershock should be similar to the mainshock. The first condition is required to assure that the propagation-path effects of the aftershock are approximately the same as that of the mainshock. The second condition does not always mean that the source mechanism of the aftershock is the same as that of the mainshock. If the S wave is dominant in observed records, the differences in the amplitude characteristic are correctable between the mechanism of the aftershock and that of the mainshock as long as the radiation from the aftershock is not nodal. In this study, we consider that the S wave was dominant in the observed records, because the records obtained were for a short distance from the source area. An aftershock (M_w 4.6, hereafter called Aftershock A) at 8:08 on March 28, 2007 occurred very near the hypocenter of the mainshock. However, the focal mechanism of this aftershock was rather different from that of the mainshock. Another aftershock (M_w = 4.0, hereafter called Aftershock B) at 15:43 on March 25, 2007 seems to have radiation characteristics similar to the mainshock, although its hypocenter was a slight distance away from the asperity area of the mainshock. Then, we examine the radiation characteristics of those two aftershocks contributing to the six stations. We estimate the displacement source spectra of both aftershocks removing

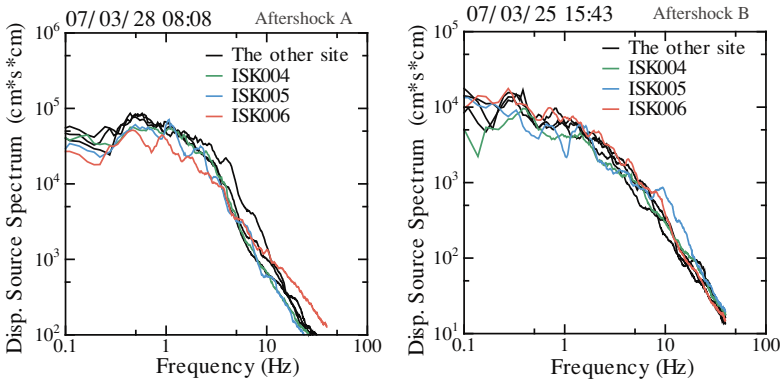

Fig. 2. The displacement source spectra of Aftershock A (left) and Aftershock B (right) estimated by observed records at six stations.

propagation-path and site effects from the observed spectrum at each station. The site effect at each station is empirically calculated, assuming that the source spectrum is given by the ω^{-2} model and the propagation-path effect is estimated by frequency-dependent Q in propagation media (Tsurugi *et al.*, 1997). We know that the radiation characteristics at low frequencies less than 1 Hz are sensitive to the focal mechanisms, but those at high frequencies are insensitive to the mechanisms because radiation characteristics are smoothed in space due to scattering effects in propagation-path (Kamae *et al.*, 1990). The displacement source spectra of Aftershock A at the stations have almost the same level in low frequencies between 0.5 and 1.0 Hz except ISK006, as shown in the right of Fig. 2. The spectral level of ISK006 is clearly lower at the low frequencies, suggesting that ISK006 is located around the nodal direction of the S wave radiation pattern. ISK006 is one of the most important points in determining the source model. It is located at the nearest station to the fault plane of the mainshock as well as southward different from other stations that are eastward from the asperity of the mainshock. Therefore, we consider that the observed records of this aftershock are not appropriate for simulating the mainshock motion using the EGF method. On the other hand, the displacement source spectra of Aftershock B at ISK006 have almost the same levels as those at ISK001, ISK002, ISK003. However, ISK004 and ISK005 have clearly a lower spectral level, as shown in the left of Fig. 2. Therefore, we used the observed records of Aftershock B as EGF for ISK001, ISK002, ISK003 and ISK006, and those of Aftershock A as EGF for ISK004 and ISK005.

4. Source Models and Synthesized Motions

4.1 Procedure

Source models of the mainshock have already been studied from the waveform inversions using teleseismic data and strong motion data by many authors (Aoi and Sekiguchi, 2007; Horikawa, 2007; Yamanaka, 2007). Almost all of these models are available for low-frequency data less than 1 Hz. Our purpose is to construct the source model for broad-band ground motions from 0.2 to 10 Hz, which is of engineering interest.

The procedure determining the source model for broad-band motions is as follows: (1) Calculate scale parameter N and stress drop ratio C from the spectral ratio CN^3 at low frequencies and CN at high frequencies between mainshock and aftershock following Irikura (1986). Generally, the source area of the mainshock is divided into $N \times N$ meshes, and the mesh size $(\Delta x) \times (\Delta w)$ is determined by the source area of the aftershock whose records are used as the empirical Green's functions. Other parameters necessary for estimating ground motions from the mainshock are given as initial values from the empirical information. (2) Infer the number of asperities and their areas. For a single asperity model, the source area of the mainshock in (1) is replaced by that of the asperity, assuming that most of the ground motions are generated from the asperity. Then, the area of the asperity is estimated to be $(N\Delta x) \times (N\Delta w)$. For a multi-asperity model, the source area of the mainshock has to be replaced by the combined areas of asperities. (3) Evaluate the agreement between the observed and synthesizes motions. Its fitting function is adopted the sum of residuals for the displacement waveforms from and residuals for acceleration envelopes (Miyake *et al.*, 1999) as follows.

$$\text{Residual values} = \sum_{\text{station}} \sum_{\text{component}} \left[\sum_t (u_{\text{obs}} - u_{\text{syn}})^2 \Big/ \left\{ \left(\sum_t u_{\text{obs}}^2 \right) \left(\sum_t u_{\text{syn}}^2 \right) \right\}^{1/2} + \sum_t \left(a_{\text{env,obs}} - a_{\text{env,syn}} \right)^2 \Big/ \left(\sum_t a_{\text{env,obs}} \right) \left(\sum_t a_{\text{env,syn}} \right) \right] \quad (1)$$

where u_{obs} and u_{syn} are the observed and the synthesized displacement waveforms, and $a_{\text{env,obs}}$ and $a_{\text{env,syn}}$ are the observed and synthesized acceleration envelopes. The weights of the residual are equal for displacement waveforms and acceleration envelopes following Miyake *et al.* (1999). The best-fit model is given from the minimum of the fitting function.

The strong ground motions synthesized using the characterized source model are largely influenced by two parameters: asperity area and stress drop on the asperity. The as-

Table 2. The range and interval of searching parameters for the grid search.

	Mesh size	Rupture velocity	Stress drop ratio	Risetime
Range of searching parameters	0.7–1.2 km	2.4–3.3 km/s	5.0–9.0	0.2–1.0 s
Interval of parameters for grid search	0.1 km	0.1 km/s	0.1	0.1 s

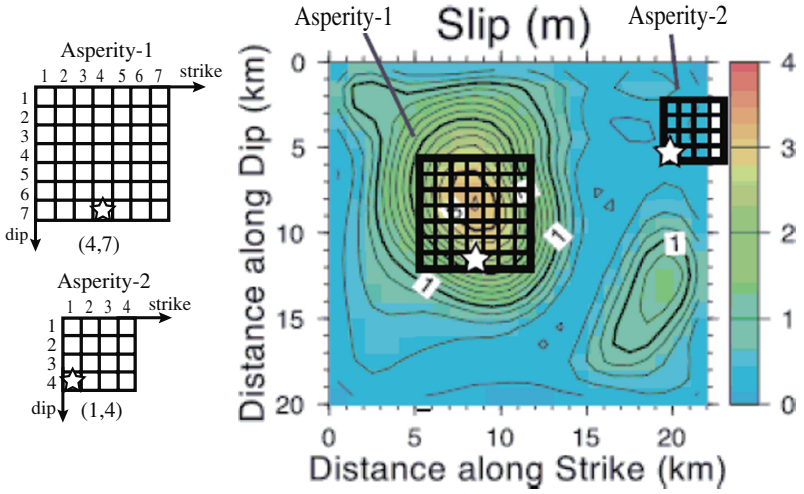

Fig. 3. Source model consisting of two asperities from forward modeling using the empirical Green's function method. Our asperity model is superimposed on the inverted slip model of Horikawa (2007). The open stars mean rupture start point.

perity area is the product of N^2 and the area of the mesh coinciding with the area of the aftershock. Fitting between the observed and synthesized waveforms at a single station has a trade-off between the asperity size and rupture velocity. The stress drop on the asperity is the product of the stress drop ratio C and the stress drop of the aftershock. The stress drop of the aftershock is estimated by the seismic moment and source area of the aftershock. Therefore, we more carefully discuss the source model, making the grid search as a parameter of the aftershock source area (coinciding with the mesh size), rupture velocity and C from a comparison between the observed and synthesized motions at ISK001, ISK002, ISK003 and ISK006 using the observed records of Aftershock B. The risetime as relatively insensitive parameters was re-estimated after the above parameters were determined. The range and interval of searching parameters for grid search are summarized in Table 2.

4.2 Result

First, we assume a single asperity model (Asperity-1) learning from the slip distribution determined using low-frequency components of strong motion data by Horikawa (2007). He carefully allocated the hypocenter and fault plane of the mainshock from the mainshock and aftershock distributions manually determined from the JMA unified data. The best-fit source model is shown in Fig. 3. The source parameters of Asperity-1 are shown in Table 3.

The scale parameter N and stress drop C were estimated to be 7 and 6.0 as an initial model from the spectral ratio between the mainshock and aftershock, respectively. The best C is estimated to be 6.3 by the grid search, keeping N constant. The length, width, risetime, and rupture velocity were determined to be 6.3 km, 6.3 km, 0.7 s, and 3.1 km/s, respectively. The rupture starting point was estimated (4, 7) as shown in the left upper of Fig. 3. Seismic moment

Table 3. The source parameters for each asperity.

	M_o (N*m)	L (km) × W (km)	$\Delta\sigma$ (MPa)
Asperity-1	2.7×10^{18}	6.3×6.3	25.8
Asperity-2	2.0×10^{17}	3.6×3.6	10.3

and stress drop were estimated to be 2.70×10^{18} N*m, 25.8 MPa, respectively. We found that the location and area of the asperity were similar to the large slip area by Horikawa (2007). The synthesized motions at the ISK001, ISK002, ISK003, and ISK006 stations are compared with observed ones in Fig. 4. The synthesized waveforms agree well with the observed ones especially in directivity pulses appearing in velocity and displacement waveforms.

On the other hand, in Fig. 4, the observed records at ISK003 have two distinct pulses in velocity waveforms, especially the NS component. The synthesized motions calculated by only Asperity-1 were not able to estimate the second pulse of observed records at ISK003. However, the second pulse does not clearly appear in the observed records at other stations. This means that the second pulse might be generated from another asperity (Asperity-2) close to ISK003. We call it the two-asperities model. We tried to obtain a better fit between the observed and synthesized velocity waveforms by putting another asperity on the fault plane near ISK003. We kept Asperity-1 that was estimated in the first trial and appended the second asperity. We assume a multi-hypocenter model for simulating ground motions. In this model, each asperity starts to break at the time when the rupture circularly propagating from the hypocenter arrives at the starting point of each asperity. The rupture velocity inside the asperity is assumed to be constant. As the result, we found the best-fit source model with two asperities

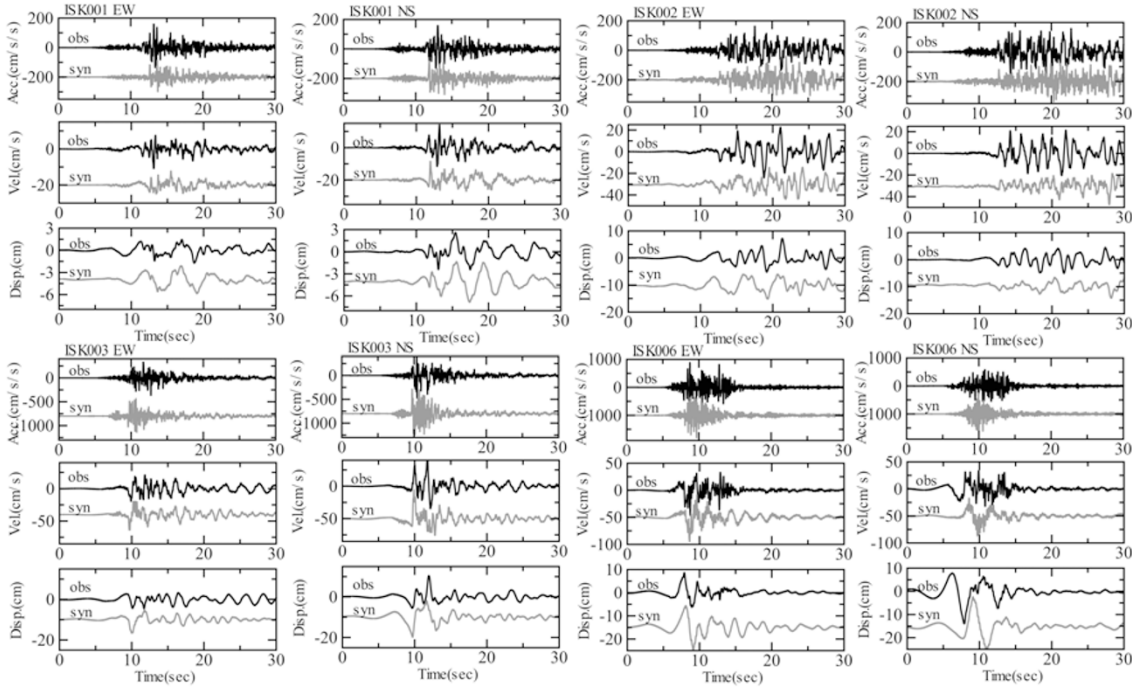

Fig. 4. Comparison between the synthesized and the observed motions at ISK001, ISK002, ISK003 and ISK006. The synthetics were made using a single asperity model (Asperity-1).

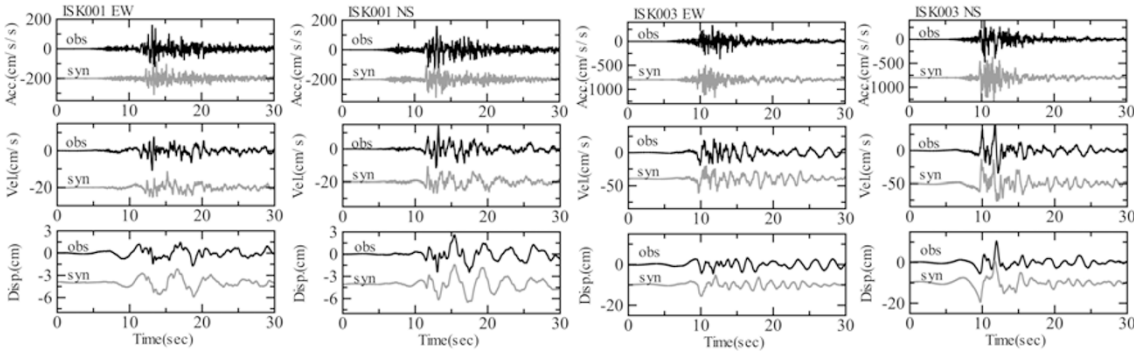

Fig. 5. Comparison between the synthesized and the observed motions at ISK001 and ISK003. The synthetics were made using two-asperities model (Asperity-1 and 2).

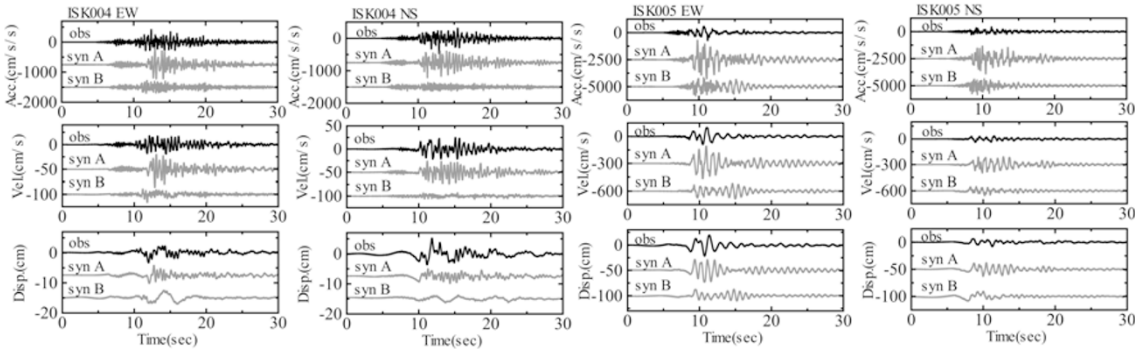

Fig. 6. Comparison between the synthesized and observed motion at ISK004 and ISK005. The synthetics were made using the two-asperities model (Asperity-1 and 2). The syn A and the syn B show the synthesized waveforms using Aftershock A and Aftershock B, respectively.

(Asperity-1 and Asperity-2), as shown in Fig. 3. Asperity-2 is located about 12 km northeast from the hypocenter. The asperity size, seismic moment, and stress drop are 13 km^2, 2.0×10^{17} N*m, 10.3 MPa, respectively. The synthesized and observed motions at ISK001 and ISK003 are compared in Fig. 5. The synthesized velocity waveform at ISK003 fits better to the observed ones. Then, we use the residual of the velocity waveforms as a fitting function. In ISK003, the

residual of the velocity is improved from 2.02 to 1.37 by adding the Asperity-2.

5. Discussion and Conclusions

We confirmed that the source model, i.e. two-asperities model, obtained above is suitable for the simulation of ground motions at other sites. We found that the observed records of Aftershock B at ISK004 and ISK005 were not appropriate for the empirical Green's functions because the radiation characteristics to both stations are relatively small compared with those to the other stations, suggesting that they are located around nodal direction. Then, we used the observed records of Aftershock A as the empirical Green's functions for estimating the ground motions at ISK004 and ISK005. The source model with the same asperity size and stress drop is adopted to synthesize the ground motions from the mainshock. Comparison between the synthesized motions and observed motions at ISK004 and ISK005 is shown in Fig. 6. The synthesized displacement using Aftershock B as EGF were underestimated in comparison with those using Aftershock A as EGF. This is consistent to the fact that ISK004 and ISK005 are located in the nodal direction, as shown in Fig. 2.

We consider that the amplitude and duration of synthesized displacement waveforms at ISK005 were similar to those of observed ones although the synthesized waveforms did not completely agree with the observed ones in individual phases. However, the synthesized acceleration and velocity were clearly overestimated. The station is underlain by very soft deposits with a thickness of about 10 m, suggesting that ground motions at this station are influenced by non-linear effects of soils near surface. On the other hand, the synthesized velocity and displacement waveforms at ISK004 do not agree well with those of observed ones, although the synthesized acceleration motions there fit the observed ones. The observed records at ISK004 might have some troubles in low frequency components.

In conclusion, our analysis shows that the source model for broad-band strong ground motions is obtained using the empirical Green's function method as long as the selection of the small event records is carefully made taking into account the radiation characteristics of the events. We confirmed that the strong motion generation areas estimated in this study coincide with the asperity area estimated from the slip model using strong motions data by Horikawa (2007).

Acknowledgments. We used the wave data provided by the K-NET of National Research Institute for Earth Science and Disaster Prevention (NIED). We also used the hypocentral information from JMA, and the moment tensor solution from the F-net (NIED). We are very grateful to Dr. Y. Fukuyama and the anonymous reviewer for reviewing the manuscript and providing valuable comments. Some figures were made using the GMT plotting package (Wessel and Smith, 1998).

References

Aoi, S. and H. Sekiguchi, Rupture process of the 2007 Noto-Hanto earthquake obtained from strong motion data, http://www.k-net.bosai.go.jp/k-net/topics/noto070325/, 2007 (in Japanese).

Earthquake Research Institute, The University of Tokyo, The Noto Hanto Earthquake in 2007, http://www.eri.u-tokyo.ac.jp/topics/noto20070325/yochiren/coco.html, 2007 (in Japanese).

Fire and Disaster Management Agency, On March 25, 2007 Noto-Hanto Earthquake, http://www.fdma.go.jp/detail/710.html, 2007 (in Japanese).

Horikawa, H., Source rupture process of 2007 Noto-Hanto Earthquake, http://unit.aist.go.jp/actfault/katsudo/jishin/notohanto/hakaikatei2.html, 2007 (in Japanese).

Irikura, K., Prediction of strong acceleration motions using empirical Green's function, *Proc. 7th Japan Earthq. Eng. Symp.*, 151–156, 1986.

Kamae, K. and K. Irikura, Source model of the 1995 Hyogo-ken Nanbu earthquake and simulation of near-source ground motion, *Bull. Seism. Soc. Am.*, **88**, 400–415, 1998.

Kamae, K., K. Irikura, and Y. Fukuchi, Prediction of strong ground motion for M7 earthquake using regional scaling relations of source parameters, *J. Struct. Constr. Eng., AIJ.*, **416**, 57–70, 1990 (in Japanese with English abstract).

Katagawa, H., M. Hamada, S. Yoshida, H. Kadosawa, A. Mitsuhashi, Y. Kono, and Y. Kinugasa, Geological development of the west sea area of the Noto peninsula district in the Neogene tertiary to quaternary, central Japan, *J. Geogr.*, **114**, 791–810, 2005.

Miyake, H., T. Iwata, and K. Irikura, Strong ground motion simulation and source modeling of the Kagoshima-ken Hokuseibu Earthquake of March 26 (M_{JMA} 6.5) and May 13 (M_{JMA} 6.3), 1997 using empirical Green's function method, *Zisin (J. Seism. Soc. Jpn.)*, **51**, 431–442, 1999.

Miyake, H., T. Iwata, and K. Irikura, Source characterization for broadband ground-motion simulation, Kinematic heterogeneous source model and strong motion generation area, *Bull. Seism. Soc. Am.*, **93**, 2531–2545, 2003.

National Research Institute for Earth Science and Disaster Prevention, NIED Seismic Moment Tensor Catalogue, http://www.fnet.bosai.go.jp, 2007.

Tsurugi, M., M. Tai, K. Irikura, and A. Kowada, Estimation of empirical site amplification effects using observed records, *Zisin*, **50**, 215–227, 1997 (in Japanese with English abstract).

Wessel, P. and W. H. F. Smith, New, improved version of Generic Mapping Tools released, *EOS*, **79**, 579, 1998.

Yamanaka, Y., EIC seismological note, **185**, http://www.eri.u-tokyo.ac.jp/sanchu/seismo Note/2007/EIC185.html, 2007 (in Japanese).

S. Kurahashi (e-mail: q05801@aitech.ac.jp), K. Masaki, and K. Irikura